ACS APPLIED MATERIALS & INTERFACES

Research Article

Cite This: ACS Appl. Mater. Interfaces 2019, 11, 17475−17481

www.acsami.org

Flexible and Highly Durable Perovskite Solar Cells with a Sandwiched Device Structure

Lili Gao, Lin Chen, Shiyu Huang, Ni Chen, and Guanjun Yang*

State Key Laboratory for Mechanical Behavior of Materials, School of Materials Science and Engineering, Xi'an Jiaotong University, Xi'an, Shaanxi 710049, PR China

Supporting Information

ABSTRACT: Flexible perovskite solar cells (PSCs) have been quickly developed as the most promising candidates for low-cost photovoltaic technology. However, the bendable and foldable properties of PSCs induce the decrease of their efficiencies. In this paper, we report the design of a new kind of flexible PSCs with a sandwiched structure. The critical layer of the flexible device is designed at a neutral layer of the sandwiched structure, which is stress-free, no matter how the device bending is. During the bending test, sandwich-structured flexible PSCs showed extremely long bending lifetime, which is at least 5−8 times higher than that of generally reported devices. At the same time, the sandwiched structure works as the encapsulation effect. The flexible device with a sandwiched structure greatly improves the device's long-term stability. Therefore, the designed sandwiched structure significantly promotes the bending ability and stability of flexible PSCs.

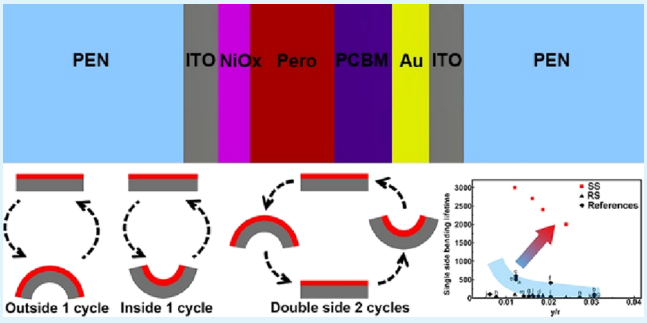

KEYWORDS: *flexible perovskite solar cells, high bending lifetime, sandwiched structure, high stability, high efficiency*

1. INTRODUCTION

Organic−inorganic hybrid perovskite solar cells (PSCs), as one of the new-fashioned photovoltaic technology, have obtained the most rapid development in power conversion efficiency (PCE).[1−8] Based on efforts of researchers, one by one records in PSCs photovoltaic field are broken, which have never been observed for other materials. With the new record of PCE beyond 23%,[9] PSCs have become the strongest rival of commercially available conventional devices such as silicon, GaAs, and CIGS.[10] Therefore, by combining high efficiency with low cost, PSCs have become the greatest potential for realizing more economically competitive solar power.[11]

Compared with other new photovoltaic devices,[12] hybrid perovskite materials possess unique crystal structures and electronic configurations, including high absorption coefficient, long carrier lifetime, high mobility, tunable band structure, and high tolerance of defects.[13−19] Based on the excellent opto-electrical properties, combining the device fabrication and material optimization, PSCs are developed rapidly and achieved high efficiency.[5,20−22] Besides the high efficiency, the stability is another issue urgently needed to be solved. Strategies have been developed to improve the stability in environment, such as mixed cations, blocking layer, and additive employing.[23,24] At the same time, researchers are also devoted to developing lead-free[25] and all-inorganic PSCs,[26] making the future of PSCs even more intriguing.

Flexible PSCs have attracted considerable attention because of their excellent characteristics such as light weight, foldablity, and bendablity. Taking the advantages of those convenient integration and versatile functionality, flexible PSCs are potential to be employed in wearable electronic and other more extensive application.[5,27−34] However, the bendability of flexible PSCs is a double-faced characteristic. Bending makes the devices undergo mechanical deformation, inducing the decrease of efficiency, which has been widely reported.[28−31,35−37] Thereby, how to utilize and evaluate properly the bending property is an important issue. So far, the most common evaluation on the bending property adopted in most literature studies is the influence of bending times on device efficiencies, which can not comprehensively and fairly evaluate the flexible bending performance. Directions on how to improve the antibending property and deep exploration on the bending failure mechanism are also primary concerns for flexible PSCs, which have always been neglected in most literature studies.

In this manuscript, we first investigate a comprehensive bending methodology to evaluate the bending property of flexible PSCs, then design a sandwich-structured (SS) flexible PSC with high bending lifetime, and deeply analyze the mechanism of the designed structure. The PSC layers are designed at the neutral layer of the device, where the plane of zero stress/strain during bending deformation. Flexible PSCs

Received: March 11, 2019
Accepted: April 25, 2019
Published: April 25, 2019

DOI: 10.1021/acsami.9b04373
ACS Appl. Mater. Interfaces 2019, 11, 17475−17481

with SS showed high bending lifetime, which is more than five times that of the generally reported devices with the routine structure (RS). The device with SS also showed excellent long-term stability than devices with RS. The flexible PSCs with SS and RS hold 86 and 49% of original efficiency, respectively, in atmospheric environment (temperature of 25 ± 5 °C, humidity of 50 ± 10%) after 500 h. In brief, the SS flexible PSCs can not only suppress the efficiency decrease during bending but also serves as the encapsulation, improving the stability of flexible PSCs.

2. RESULTS AND DISCUSSION

2.1. Bending Methodology of the Perovskite Film on the Flexible Substrate. Generally, bending refers to the ability to deform, either for materials or for devices. We propose three common and acceptable standard evaluation methodologies, bending directions, bending cycles, and bending angle (corresponding to radius of curvature), which determine the bending properties of solar cells.

Bending directions can be divided into single-side bending and double-side bending. Single-side bending can be further divided into outside bending and inside bending, as the schematic diagram shown in Figure 1a–c. Outside or inside

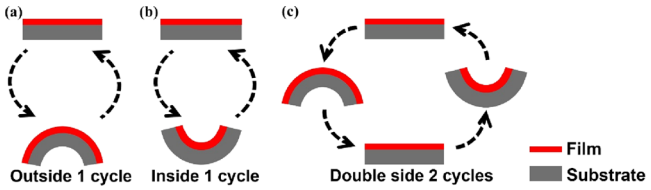

Figure 1. Definition of (a) one cycle of outside bending, (b) one cycle of inside bending, and (c) two cycles of double side bending.

bending bares one cycle; however, double-side bending bares two cycles with once inside bending and once outside bending. Different bending directions will induce film failing by different loads such as tension or compression. In order to detect the influence of bending on film morphology, we first prepared a perovskite film on the flexible substrate by the reported gas pump method,[38] and then bent them using the home-made bending machine as shown in Figure S1. The bending angle is set as 90° and bending cycles are set as 10 000 and 20 000 for single-side and double-side bending, respectively. The bending results of films morphologies are shown in Figure S2. When the film is bent outside, it would bear tension, when the film is bent inside, it would bear compression. Tension and compression are equal in value but opposite in direction. Tension usually leads to cracks in the film and compression makes the film spalling from the substrate. The film bending at double side bears both tension and compression alternately, inducing deeper cracks and quicker spallation. The bared stress during the bending process can be calculated based on eq 1, where σ and ε are stress and strain, respectively. E is elasticity modulus. ε is related to the bending radius and neutral layer; as the schematic diagram shown in Figure 2, the relationship can be deduced as eq 2.

$$\sigma = E \cdot \varepsilon \tag{1}$$

$$\varepsilon = \frac{\left(l + \frac{h_1}{2} + h_2 + R - l\right)\cdot 2\theta - l\cdot 2\theta}{l\cdot 2\theta} = \frac{\frac{h_1}{2} + h_2 + R - l}{l} \approx \frac{\frac{h_1}{2} + h_2}{R} \tag{2}$$

$$R = \frac{L}{2\theta} \tag{3}$$

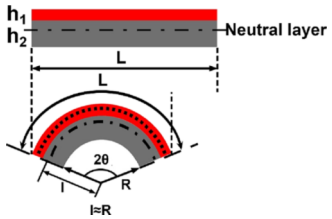

Figure 2. Schematic diagram for strain deduction.

The bending angle is another methodology to evaluate bending deformation. As shown in Figure 2, the bending angle is relevant with the bending radius and film length. In this manuscript, the film length is 8 mm. The relationship of the bending radius and bending angle can be described as eq 3. A series of bending angles and radii are shown in Table S1. From eq 2, strain increases with the decrease of the bending radius, producing more cracks. We set perovskite film bending double side 30 000 cycles at different angles, and the film morphologies are shown in Figure S3a–d. As the results show, with the increase of the bending angle, the number of cracks increases and the depth of cracks is more serious. Therefore, bending with a small angle will reduce damage.

Finally, the bending cycle is another important bending methodology. Actually, the bending cycle is related to the fatigue test for a material. As shown in Figure S4a–d, we bent perovskite films double side at 90° with different cycles. With bending cycles increasing, crack numbers increase and the vertical cracks become more deep. Furthermore, when double-side bending cycle increases to 60 000, the film presents transverse cracks besides vertical cracks. There even exist small cracks along grain boundaries between large cracks, as shown in Figure S5a. Finally, the films fall off because of fatigue as illustrated in Figure S5b. Thereby, bending fatigue is also an important failure mode.

Based on the above discussion, bending directions, bending angles, and bending cycles are the three main bending methodologies. Rational controlling bending directions, bending radius, and bending cycles are of critical importance for improving flexible device bending lifetime.

2.2. Improved Bending Lifetime of SS Devices at Different Bending Modes. In order to test the bending performance of flexible PSCs, the devices were fabricated with two kinds of different structures, as shown in Figure 3a. RS is polyethylene terephthalate (PEN)/indium-doped tin oxide (ITO)/NiO_x/PVSK/PCBM/Ag, SS has another piece of ITO/PEN at the side of Ag. The perovskite layer of SS is located at the neutral layer of the device structure. The initial efficiency of the flexible PSC with SS is 12.81% with an active area of 0.15 cm^2, as the J–V curve shown in Figure 3b. The forward and reverse scans are shown in Figure S6. Similar efficiencies of devices with RS and SS are shown in Figure S7. Then, we conducted the bending test of them with double-side bending

DOI: 10.1021/acsami.9b04373
ACS Appl. Mater. Interfaces 2019, 11, 17475–17481

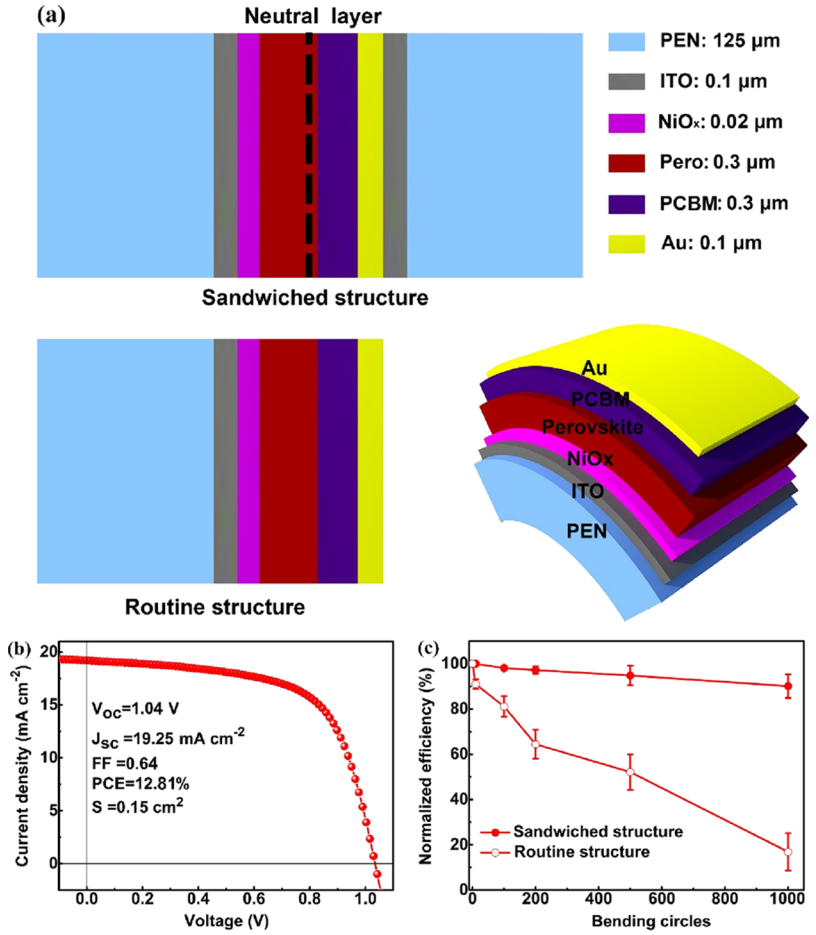

Figure 3. (a) Schematic diagram of different device structures, (b) $J-V$ curve of flexible PSC with SS, (c) efficiency damage of two kinds of the device structure after double-side bending 2000 cycles at 45°.

2000 cycles at 45°. The result shows that the SS device holds 97% of original efficiency; however, the efficiency of the RS device has dropped to 20% of original efficiency, as shown in Figure 3c. The slight decrease of the SS device efficiency may be a result of the error of PEN thickness. Thereby, we can conclude that the SS can significantly improve the antibending ability of flexible PSCs.

In order to measure the performance of RS and SS solar cells, we further compared these two kinds of devices at different bending methodologies. As shown in Figure 4a, both double-side and single-side bending, outputting performances of SS devices are almost consistent with original performances after bending 2000 cycles at 90° bending angle. Comparatively, the performances of RS devices dropped quickly, and the efficiency decreased nearly to zero after 2000 cycles bending. With the bending cycles increasing, the performances of RS devices dropped quickly before 300 bending cycles, then tended to decrease slowly. Furthermore, with the increase of the bending angle, performances of RS devices degraded significantly compared with SS devices after double-side bending 1000 cycles, as shown in Figure 4b. Based on eq 3, large bending angle means small radius of curvature, thereby, the strain and stress are enlarged, inducing the device damage quickly. In addition, normalized efficiencies of the two kinds of devices were researched with bending cycles increasing with different bending radius. The single-side and double-side bending results are shown in Figure 4c,d, respectively. Both double-side and single-side bending with large bending radius induce quick and huge decrease of efficiency. Double-side bending decreased more seriously than single-side bending because of the alternate action of tension and compression.

All the decreased curves of device performances and bending cycles can be concluded as an exponential function, as shown in the following equation

$$\eta = A\, e^{-c} + B \tag{4}$$

where η is normalized efficiency, c is bending cycle, A and B are constants depending on the bending mode, bending degree, and bending resistance of devices. Based on the formula, we can accurately deduce the remaining efficiency at corresponding bending cycles for any kind of flexible device bending. We define 90% original efficiency bared bending cycles as the device bending lifetime. Subsequently, we compared the bending lifetime at different bending degrees of our results and other reports, as shown in Figure 5. The detailed figures are summarized in Table S2. From the comparison, the bending lifetime of SS devices is at least five to eight times higher than the general structure device. It can be concluded that SS can significantly improve the device bending lifetime.

Besides the improved bending lifetime, SS devices also showed better long-term stability than RS devices. The PEN on the side of the Ag layer serves as the encapsulation layer to protect the invading of environment. Just as shown in Figure S8, after 500 h measurement in atmospheric environment (temperature 25 ± 5 °C, humidity 40 ± 10%), the SS flexible device retains 86% of original efficiency, while the compared

DOI: 10.1021/acsami.9b04373
ACS Appl. Mater. Interfaces 2019, 11, 17475−17481

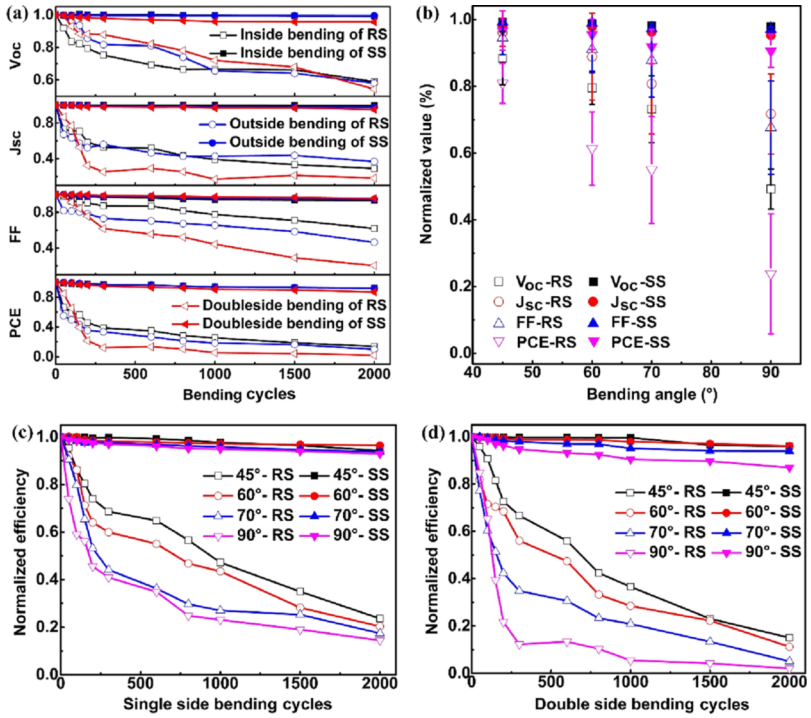

Figure 4. Device performance of two kinds of devices at different bending conditions, (a) bending cycles with different bending directions at 90° bending angle, (b) bending angle with double-side bending 1000 cycles, (c) single-side bending at different bending angles, (d) double-side bending at different bending angles.

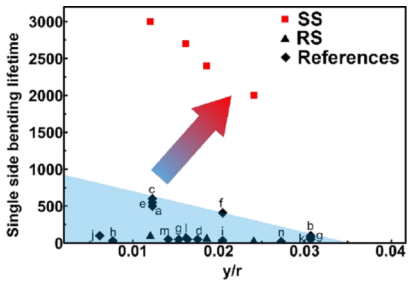

Figure 5. Relationship of bending lifetimes and bending degree, y is the distance to neutral layer, r is bending radius, a,[39] b,[40] c,[41] d,[42] e,[43] f,[44] g,[45] h,[46] i,[47] j,[48] k,[49] l,[50] m,[51] n.[38]

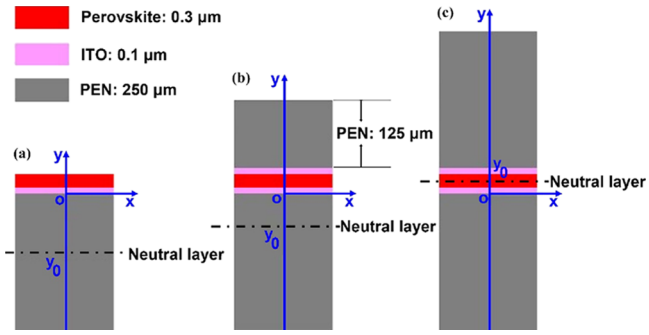

Figure 6. Schematic diagram of the perovskite film under different locations of the film structure, (a) perovskite layer is located at the top of an ITO-coated PEN, (b) perovskite layer is located at the middle of two pieces of ITO-coated PEN with different thickness, (c) perovskite layer is located at the middle of two pieces of ITO-coated PEN with the same thickness.

RS device efficiency drops to 49% of original efficiency. Therefore, the flexible devices with SS can not only improve the bending lifetime but also the stability of flexible devices.

2.3. Mechanism of SS for Improved Device Lifetime.

In order to clarify the mechanism of SS devices with improved bending lifetime, we analyze the structure from the mechanics. From the structural mechanics, we know that the neutral layer is the plane that will not bear any force no matter how bending stress and strain are. The neutral layer of a structure can be confirmed based on eq 5. E_i is the elasticity modulus of the i layer, h_i is the thickness of the i layer, and y_i is the distance of the centroid in the i layer to the origin of the coordinate axis, respectively. As the schematic diagram shown in Figure 6, we design the perovskite layer at different structures and calculate the location of the neutral layer. Elasticity modulus of PEN and ITO has been reported as 5.3 ± 0.2 and 185 ± 5 GPa, respectively.[52,53] We measured the elasticity modulus of perovskite using nanoindentation. As shown in Figure S9a, we first prepared the single crystal of $CH_3NH_3PbI_3$ using the inverse solubility at high temperatures in γ-butyrolactone[54] and then measured by nanoindentation. The curves of load and depth are shown in Figure S9b, and the elasticity modulus of $CH_3NH_3PbI_3$ is 17.3 ± 0.5 GPa. Thereby, based on eq 5, we calculated the neutral layers y_0 are −122.80, −44.71, and 0 μm for the structures of a, b, and c in Figure 6, respectively. Based on the structural mechanics, the neutral layer will not bear stress, and the position more far to the neutral layer will bear more stress. Therefore, the perovskite layer in Figure 6a bears the most serious stress, the layer in Figure 6b bears slight stress, and the layer in Figure 6c does not bear any stress no matter how bent it is. In order to further confirm the result, three kinds of perovskite films were prepared just as the module in Figure 6a−c and bended them at 45° double-side 20 000 cycles. The perovskite layers show a very different morphology as shown in Figure S10. Figure S10a−c shows the morphologies of modules in Figure 6a−c, respectively. The

DOI: 10.1021/acsami.9b04373
ACS Appl. Mater. Interfaces 2019, 11, 17475−17481

perovskite layer with 122.80 μm to the neutral layer is damaged seriously with deep cracks, the perovskite layer with 44.71 μm to the neutral layer shows slight cracks, and the one just in the neutral layer shows perfect compact morphology. Thereby, the flexible devices with SS can process more greatly bending lifetime.

Actually, during the production of PEN, there is always unavoidable thickness error. The error is usually within 3 μm. Because of the thickness error, the perovskite layer is not always located at the neutral layer. Based on eqs 2 and 3, we deduced the relationship of perovskite film bared strain and bending angles for the three kinds of conditions discussed above, as shown in Figure 7. Structure a in Figure 6 showed the

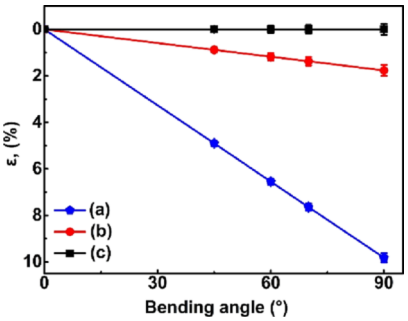

Figure 7. Relationship of perovskite film bared strain at different bending angles with three kinds of structures, (a) structure shown in Figure 6a, (b) structure shown in Figure 6b, and (c) structure shown in Figure 6c.

largest strain, and structure c showed the minimum strain. Even though the thickness error of PEN induced some shift of the neutral layer, the perovskite film bared strain in structure c is still the minimum. All the strain induced by the thickness error is shown as a line in Figure 7. Thereby, the SS structure is the best to protect the PSC layers from damage during the bending process.

$$y_0 = \frac{\sum E_i h_i y_i}{\sum E_i h_i} \tag{5}$$

In addition, based on the relationship of stress and strain as shown in eqs 1 and 2, we can estimate the stress condition of flexible PSCs and design a suitable structure to improve device bending lifetime. As shown in Figure S11a, it shows the relationship of strain of the layer distance to the neutral layer. Furthermore, based on the estimation of the bared strain from Figure S11a, the layer can be estimated as the most bared bending cycles until devices damage, as shown in Figure S11b. Thereby, we can pre-estimate the failure condition of the flexible devices, which is a meaningful guidance for applications.

3. CONCLUSIONS

In conclusion, we comprehensively investigate the methodologies to evaluate bending of flexible PSCs and designed a new kind of SS flexible PSC with a high bending lifetime. The device layers are designed on the neutral layer of the SS, which is not forced no matter how the device bends. Therefore, after double-side bending for 2000 cycles at 45°, the SS device still holds 97% of original efficiency, while the RS device drops to 20% of original efficiency. Compared with general device bending, SS devices show five to eight times higher bending lifetime. Besides, the SS works as the encapsulation effect, which greatly improves the long-time stability. The SS flexible device can still hold 86% original efficiency after 500 h in atmospheric environment (temperature 25 ± 5 °C, humidity 40 ± 10%), while RS device efficiency has dropped to 49% of original efficiency. Thereby, the designed sandwiched device structure significantly improved the practical application of flexible PSCs.

4. EXPERIMENTS

4.1. Materials Preparation. Lead iodide (PbI_2, 99.99%), iodine methylamine (CH_3NH_3I), and PCBM were purchased from Xi'an Polymer Light Technology Corp. *N*,*N*-dimethylformamide (DMF, 99.8%), dimethyl sulfoxide (DMSO, 99.8%), and chlorobenzene were purchased from National Drug Group Chemical Reagents Co., Ltd. All the materials were used as received.

4.2. Device Fabrication. ITO-PEN sheets (40 Ω/cm^2) were rinsed successively with ethyl alcohol, deionized water in an ultrasonic bath for 15 min, and blow-dried by nitrogen. The flexible substrate was mounted onto a rigid glass substrate for easy device fabrication. Before the sputtering of NiO_x, the ITO-PEN was treated with ozone and ultraviolet for 20 min for the interface contacting. The hole transporting layer, NiO_x, was prepared by rapid plasma deposition with the thickness of 20 nm. The perovskite film was prepared by the reported gas pump drying method.[38] The solvent is DMSO and DMF with a volume rate of 1:9. The precursor solution was 1 mol/L with PbI_2 and CH_3NH_3I with molar rate of 1:1. After spin-coating by 2000 rpm 7 s, the liquid thin film was dried by gas pump, and the dried mirror-black thin film was heated at the hot plate for 10 min. Then, the electron transport layer, PCBM, was spin-coated at 3000 rpm for 30 s. PCBM was dissolved in chlorobenzene with the concentration of 20 mg/mL. Finally, Ag was evaporated, as the electrode, with a thickness of 100 nm. Devices with SS was coated with another ITO-PEN sheet by thermocompression using the Surlyn film at 80 °C.

4.3. Characterization. The scanning electron microscopy (SEM) morphologies were measured by a field-emission scanning electron microscope (MIRA 3LMH, TESCAN, Czech Republic). The elasticity modulus of perovskite single crystal was measured by nanomechanical metrology techniques (Hysitron, Inc.). The *J*−*V* curves (reverse and forward) were measured with a 2400 series source meter, Keithley Instruments, under the illumination of simulated air-mass 1.5 sunlight at 100 mW cm^{-2} (Class AAA solar Sol3A, Oriel Instruments). The steady-state current densities and the PCE of the devices were measured at the maximum power point. The bending test was carried out by a home-developed flexible solar cell bending tester, by which the bending conditions, including bending directions, bending radius, and bending cycles, were accurately controlled with high reproducibility of every bending results.

■ ASSOCIATED CONTENT

Supporting Information

The Supporting Information is available free of charge on the ACS Publications website at DOI: 10.1021/acsami.9b04373.

Bending machine; films morphologies bending at different directions, different angles, and different cycles; *J*−*V* curves of flexible PSCs; stability of two kinds of device structure; photos of single crystal of $CH_3NH_3PbI_3$; curves of load and depth to get elasticity modulus of $CH_3NH_3PbI_3$; table of bending radius and bending angles conversion; and table of comparison of flexible solar cells reported in some papers (PDF)

■ AUTHOR INFORMATION

Corresponding Author

*E-mail: ygj@mail.xjtu.edu.cn.

DOI: 10.1021/acsami.9b04373
ACS Appl. Mater. Interfaces 2019, 11, 17475−17481

ORCID

Guanjun Yang: 0000-0002-7753-3636

Notes

The authors declare no competing financial interest.

■ ACKNOWLEDGMENTS

The authors thank the financial support of the National Program for Support of Top-notch Young Professionals.

■ REFERENCES

(1) Im, J.-H.; Jang, I.-H.; Pellet, N.; Grätzel, M.; Park, N.-G. Growth of $CH_3NH_3PbI_3$ cuboids with controlled size for high-efficiency perovskite solar cells. *Nat. Nanotechnol.* **2014**, *9*, 927−932.

(2) Yang, M.; Zhang, T.; Schulz, P.; Li, Z.; Li, G.; Kim, D. H.; Guo, N.; Berry, J. J.; Zhu, K.; Zhao, Y. Facile fabrication of large-grain $CH_3NH_3PbI_{3-x}Br_x$ films for high-efficiency solar cells via CH_3NH_3Br-selective Ostwald ripening. *Nat. Commun.* **2016**, *7*, 12305.

(3) Gao, L.-L.; Li, C.-X.; Li, C.-J.; Yang, G.-J. Large-area high-efficiency perovskite solar cells based on perovskite films dried by the multi-flow air knife method in air. *J. Mater. Chem. A* **2017**, *5*, 1548−1557.

(4) Gao, L.; Huang, S.; Chen, L.; Li, X. L.; Ding, B.; Huang, S. Y.; Yang, G. J. Excellent Stability of Perovskite Solar Cells by Passivation Engineering. *Sol. RRL* **2018**, *2*, 1870194.

(5) Ginting, R. T.; Jeon, E.-B.; Kim, J.-M.; Jin, W.-Y.; Kang, J.-W. Dual Light Trapping and Water-Repellent Effects of a Flexible-Based Inverse Micro-Cone Array for Organic and Perovskite Solar Cells. *ACS Appl. Mater. Interfaces* **2018**, *10*, 31291−31299.

(6) Hou, Q.; Ren, J.; Chen, H.; Yang, P.; Shao, Q.; Zhao, M.; Zhao, X.; He, H.; Wang, N.; Luo, Q.; Guo, Z. Synergistic Hematite-Fullerene Electron-Extracting Layers for Improved Efficiency and Stability in Perovskite Solar Cells. *ChemElectroChem* **2018**, *5*, 726−731.

(7) Yang, L.; Wang, X.; Mai, X.; Wang, T.; Wang, C.; Li, X.; Murugadoss, V.; Shao, Q.; Angaiah, S.; Guo, Z. Constructing efficient mixed-ion perovskite solar cells based on TiO_2 nanorod array. *J. Colloid Interface Sci.* **2019**, *534*, 459−468.

(8) Bella, F.; Galliano, S.; Piana, G.; Giacona, G.; Viscardi, G.; Grätzel, M.; Barolo, C.; Gerbaldi, C. Boosting the efficiency of aqueous solar cells: A photoelectrochemical estimation on the effectiveness of TiCl4 treatment. *Electrochim. Acta* **2019**, *302*, 31−37.

(9) Jiang, Q.; Zhao, Y.; Zhang, X.; Yang, X.; Chen, Y.; Chu, Z.; Ye, Q.; Li, X.; Yin, Z.; You, J. Surface passivation of perovskite film for efficient solar cells. *Nat. Photonics* **2019**, DOI: 10.1038/s41566-019-0398-2.

(10) Bush, K. A.; Palmstrom, A. F.; Yu, Z. S. J.; Boccard, M.; Cheacharoen, R.; Mailoa, J. P.; McMeekin, D. P.; Hoye, R. L. Z.; Bailie, C. D.; Leijtens, T.; Peters, I. M.; Minichetti, M. C.; Rolston, N.; Prasanna, R.; Sofia, S.; Harwood, D.; Ma, W.; Moghadam, F.; Snaith, H. J.; Buonassisi, T.; Holman, Z. C.; Bent, S. F.; McGehee, M. D. 23.6%-efficient monolithic perovskite/silicon tandem solar cells with improved stability. *Nat. Energy* **2017**, *2*, 17009.

(11) Abate, A.; Correa-Baena, J.-P.; Saliba, M.; Su'ait, M. S.; Bella, F. Perovskite Solar Cells: From the Laboratory to the Assembly Line. *Chem.—Eur. J.* **2018**, *24*, 3083−3100.

(12) Bella, F.; Popovic, J.; Lamberti, A.; Tresso, E.; Gerbaldi, C.; Maier, J. Interfacial Effects in Solid-Liquid Electrolytes for Improved Stability and Performance of Dye-Sensitized Solar Cells. *ACS Appl. Mater. Interfaces* **2017**, *9*, 37797−37803.

(13) Chen, J.; Seo, J.-Y.; Park, N.-G. Simultaneous improvement of photovoltaic performance and stability by in situ formation of 2D perovskite at $(FAPbI_3)$ 0.88 $(CsPbBr_3)$ 0.12/CuSCN interface. *Adv. Energy Mater.* **2018**, *8*, 1702714.

(14) Jiang, Q.; Chu, Z.; Wang, P.; Yang, X.; Liu, H.; Wang, Y.; Yin, Z.; Wu, J.; Zhang, X.; You, J. Planar-Structure Perovskite Solar Cells with Efficiency beyond 21. *Adv. Mater.* **2017**, *29*, 1703852.

(15) Heo, J. H.; Song, D. H.; Han, H. J.; Kim, S. Y.; Kim, J. H.; Kim, D.; Shin, H. W.; Ahn, T. K.; Wolf, C.; Lee, T. W.; Im, S. H. Planar $CH_3NH_3PbI_3$ Perovskite Solar Cells with Constant 17.2% Average Power Conversion Efficiency Irrespective of the Scan Rate. *Adv. Mater.* **2015**, *27*, 3424−3430.

(16) Jeon, Y.-J.; Lee, S.; Kang, R.; Kim, J. E.; Yeo, J. S.; Lee, S. H.; Kim, S. S.; Yun, J. M.; Kim, D. Y. Planar heterojunction perovskite solar cells with superior reproducibility. *Sci. Rep.* **2015**, *4*, 6953.

(17) Jiang, Q.; Yan, L.; Liu, C.; Liu, C.; Guo, Z. Mesoporous TiO_2 Vacancies Modification for Halide Perovskite Solar Cells. *Eng. Sci.* **2018**, *1*, 64−68.

(18) Tavakoli, M. M.; Prochowicz, D.; Yadav, P.; Tavakoli, R.; Saliba, M. Zinc Stannate Nanorod as an Electron Transporting Layer for Highly Efficient and Hysteresis-less Perovskite Solar Cells. *Eng. Sci.* **2018**, *3*, 48−53.

(19) Xu, T.; Kong, D.; Xi, Z.; Huang, T.; Wu, H.; Kou, K.; Wang, R.; Chen, L.; Ma, T. Photoinduced Polyacrylate Based Polymer Electrolyte for Quasi-solid State Dye Sensitized Solar Cell Application. *Eng. Sci.* **2019**, *6*, 001.

(20) Ke, W.; Fang, G.; Wan, J.; Tao, H.; Liu, Q.; Xiong, L.; Qin, P.; Wang, J.; Lei, H.; Yang, G.; Qin, M.; Zhao, X.; Yan, Y. Efficient hole-blocking layer-free planar halide perovskite thin-film solar cells. *Nat. Commun.* **2015**, *6*, 6700.

(21) Kim, M.; Kim, G.-H.; Oh, K. S.; Jo, Y.; Yoon, H.; Kim, K.-H.; Lee, H.; Kim, J. Y.; Kim, D. S. High-Temperature-Short-Time Annealing Process for High-Performance Large-Area Perovskite Solar Cells. *ACS Nano* **2017**, *11*, 6057−6064.

(22) Son, D.-Y.; Lee, J.-W.; Choi, Y. J.; Jang, I.-H.; Lee, S.; Yoo, P. J.; Shin, H.; Ahn, N.; Choi, M.; Kim, D.; Park, N.-G. Self-formed grain boundary healing layer for highly efficient $CH_3NH_3PbI_3$ perovskite solar cells. *Nat. Energy* **2016**, *1*, 16081.

(23) Hwang, H.; Park, S.; Heo, J. H.; Kim, W.; Ahn, H.; Kim, T.-S.; Im, S. H.; Son, H. J. Enhancing performance and stability of perovskite solar cells using hole transport layer of small molecule and conjugated polymer blend. *J. Power Sources* **2019**, *418*, 167−175.

(24) Qin, K.; Dong, B.; Wang, S. Improving the stability of metal halide perovskite solar cells from material to structure. *J. Energy Chem.* **2019**, *33*, 90−99.

(25) Ke, W.; Stoumpos, C. C.; Kanatzidis, M. G. "Unleaded" Perovskites: Status Quo and Future Prospects of Tin-Based Perovskite Solar Cells. *Adv. Mater.* **2018**, No. e1803230.

(26) Bella, F.; Renzi, P.; Cavallo, C.; Gerbaldi, C. Caesium for Perovskite Solar Cells: An Overview. *Chem.—Eur. J.* **2018**, *24*, 12183−12205.

(27) Qin, P.-L.; He, Q.; Chen, C.; Zheng, X. L.; Yang, G.; Tao, H.; Xiong, L. B.; Xiong, L.; Li, G.; Fang, G. J. High-Performance Rigid and Flexible Perovskite Solar Cells with Low-Temperature Solution-Processable Binary Metal Oxide Hole-Transporting Materials. *Sol. RRL* **2017**, *1*, 1700058.

(28) Wang, C.; Guan, L.; Zhao, D.; Yu, Y.; Grice, C. R.; Song, Z.; Awni, R. A.; Chen, J.; Wang, J.; Zhao, X.; Yan, Y. Water Vapor Treatment of Low-Temperature Deposited SnO_2 Electron Selective Layers for Efficient Flexible Perovskite Solar Cells. *ACS Energy Lett.* **2017**, *2*, 2118−2124.

(29) Liu, X.; Guo, X.; Lv, Y.; Hu, Y.; Lin, J.; Fan, Y.; Zhang, N.; Liu, X. Enhanced Performance and Flexibility of Perovskite Solar Cells Based on Microstructured Multilayer Transparent Electrodes. *ACS Appl. Mater. Interfaces* **2018**, *10*, 18141−18148.

(30) Xiong, H.; DeLuca, G.; Rui, Y.; Zhang, B.; Li, Y.; Zhang, Q.; Wang, H.; Reichmanis, E. Modifying Perovskite Films with Polyvinylpyrrolidone for Ambient-Air-Stable Highly Bendable Solar Cells. *ACS Appl. Mater. Interfaces* **2018**, *10*, 35385−35394.

(31) Jin, S. W.; Lee, Y. H.; Yeom, K. M.; Yun, J.; Park, H.; Jeong, Y. R.; Hong, S. Y.; Lee, G.; Oh, S. Y.; Lee, J. H.; Noh, J. H.; Ha, J. S. Highly Durable and Flexible Transparent Electrode for Flexible Optoelectronic Applications. *ACS Appl. Mater. Interfaces* **2018**, *10*, 30706−30715.

(32) Heo, J. H.; Shin, D. H.; Lee, M. L.; Kang, M. G.; Im, S. H. Efficient Organic−Inorganic Hybrid Flexible Perovskite Solar Cells Prepared by Lamination of Polytriarylamine/$CH_3NH_3PbI_3$/Anodized

Ti Metal Substrate and Graphene/PDMS Transparent Electrode Substrate. *ACS Appl. Mater. Interfaces* **2018**, *10*, 31413−31421.
(33) Chen, C.; Li, H.; Ding, X.; Cheng, M.; Li, H.; Xu, L.; Qiao, F.; Li, H.; Sun, L. Molecular Engineering of Triphenylamine-Based Non-Fullerene Electron-Transport Materials for Efficient Rigid and Flexible Perovskite Solar Cells. *ACS Appl. Mater. Interfaces* **2018**, *10*, 38970−38977.
(34) Chen, H.; Liu, T.; Wang, B.; Liu, Z.; Li, Y.; Zhao, Q.; Wang, N.; He, H.; Liu, H.; Guo, Z. Highly efficient charge collection in dye-sensitized solar cells based on nanocomposite photoanode filled with indium-tin oxide interlayer. *Adv. Compos. Hybrid. Mater.* **2018**, *1*, 356−363.
(35) Xu, M.; Feng, J.; Fan, Z.-J.; Ou, X.-L.; Zhang, Z.-Y.; Wang, H.-Y.; Sun, H.-B. Flexible perovskite solar cells with ultrathin Au anode and vapour-deposited perovskite film. *Sol. Energy Mater. Sol. Cells* **2017**, *169*, 8−12.
(36) Le, K.; Wang, Z.; Wang, F.; Wang, Q.; Shao, Q.; Murugadoss, V.; Wu, S.; Liu, W.; Liu, J.; Gao, Q.; Guo, Z. Sandwich-like NiCo layered double hydroxide/reduced graphene oxide nanocomposite cathodes for high energy density asymmetric supercapacitors. *Dalton Trans.* **2019**, *48*, 5193−5202.
(37) Luo, Q.; Ma, H.; Hou, Q.; Li, Y.; Ren, J.; Dai, X.; Yao, Z.; Zhou, Y.; Xiang, L.; Du, H.; He, H.; Wang, N.; Jiang, K.; Lin, H.; Zhang, H.; Guo, Z. All-Carbon-Electrode-Based Endurable Flexible Perovskite Solar Cells. *Adv. Funct. Mater.* **2018**, *28*, 1706777.
(38) Gao, L.-L.; Liang, L.-S.; Song, X.-X.; Ding, B.; Yang, G.-J.; Fan, B.; Li, C.-X.; Li, C.-J. Preparation of flexible perovskite solar cells by a gas pump drying method on a plastic substrate. *J. Mater. Chem. A* **2016**, *4*, 3704−3710.
(39) Wang, C.; Guan, L.; Zhao, D.; Yu, Y.; Grice, C. R.; Song, Z.; Awni, R. A.; Chen, J.; Wang, J.; Zhao, X.; Yan, Y. Water Vapor Treatment of Low-Temperature Deposited SnO_2 Electron Selective Layers for Efficient Flexible Perovskite Solar Cells. *ACS Energy Lett.* **2017**, *2*, 2118−2124.
(40) Heo, J. H.; Shin, D. H.; Jang, M. H.; Lee, M. L.; Kang, M. G.; Im, S. H. Highly flexible, high-performance perovskite solar cells with adhesion promoted $AuCl_3$-doped graphene electrodes. *J. Mater. Chem. A* **2017**, *5*, 21146−21152.
(41) Jung, J. W.; Park, J.-S.; Han, I. K.; Lee, Y.; Park, C.; Kwon, W.; Park, M. Flexible and highly efficient perovskite solar cells with a large active area incorporating cobalt-doped poly(3-hexylthiophene) for enhanced open-circuit voltage. *J. Mater. Chem. A* **2017**, *5*, 12158−12167.
(42) Jung, K.; Lee, J.; Kim, J.; Chae, W.-S.; Lee, M.-J. Solution-processed flexible planar perovskite solar cells: A strategy to enhance efficiency by controlling the ZnO electron transfer layer, PbI_2 phase, and $CH_3NH_3PbI_3$ morphologies. *J. Power Sources* **2016**, *324*, 142−149.
(43) Park, M.; Kim, J.-Y.; Son, H. J.; Lee, C.-H.; Jang, S. S.; Ko, M. J. Low-temperature solution-processed Li-doped SnO_2 as an effective electron transporting layer for high-performance flexible and wearable perovskite solar cells. *Nano Energy* **2016**, *26*, 208−215.
(44) Park, M.; Park, J.-S.; Han, I. K.; Oh, J. Y. High-performance flexible and air-stable perovskite solar cells with a large active area based on poly(3-hexylthiophene) nanofibrils. *J. Mater. Chem. A* **2016**, *4*, 11307−11316.
(45) Heo, J. H.; Lee, M. H.; Han, H. J.; Patil, B. R.; Yu, J. S.; Im, S. H. Highly efficient low temperature solution processable planar type $CH_3NH_3PbI_3$ perovskite flexible solar cells. *J. Mater. Chem. A* **2016**, *4*, 1572−1578.
(46) Chen, C.; Cheng, Y.; Dai, Q.; Song, H. Radio Frequency Magnetron Sputtering Deposition of TiO_2 Thin Films and Their Perovskite Solar Cell Applications. *Sci. Rep.* **2016**, *5*, 17684.
(47) Lee, M.; Jo, Y.; Kim, D. S.; Jeong, H. Y.; Jun, Y. Efficient, durable and flexible perovskite photovoltaic devices with Ag-embedded ITO as the top electrode on a metal substrate. *J. Mater. Chem. A* **2015**, *3*, 14592−14597.
(48) Dianetti, M.; Di Giacomo, F.; Polino, G.; Ciceroni, C.; Liscio, A.; D'Epifanio, A.; Licoccia, S.; Brown, T. M.; Di Carlo, A.; Brunetti, F. TCO-free flexible organo metal trihalide perovskite planar-heterojunction solar cells. *Sol. Energy Mater. Sol. Cells* **2015**, *140*, 150−157.
(49) Kim, B. J.; Kim, D. H.; Lee, Y.-Y.; Shin, H.-W.; Han, G. S.; Hong, J. S.; Mahmood, K.; Ahn, T. K.; Joo, Y.-C.; Hong, K. S.; Park, N.-G.; Lee, S.; Jung, H. S. Highly efficient and bending durable perovskite solar cells: toward a wearable power source. *Energy Environ. Sci.* **2015**, *8*, 916−921.
(50) Wang, X.; Li, Z.; Xu, W.; Kulkarni, S. A.; Batabyal, S. K.; Zhang, S.; Cao, A.; Wong, L. H. TiO_2 nanotube arrays based flexible perovskite solar cells with transparent carbon nanotube electrode. *Nano Energy* **2015**, *11*, 728−735.
(51) Dkhissi, Y.; Huang, F.; Rubanov, S.; Xiao, M.; Bach, U.; Spiccia, L.; Caruso, R. A.; Cheng, Y.-B. Low temperature processing of flexible planar perovskite solar cells with efficiency over 10%. *J. Power Sources* **2015**, *278*, 325−331.
(52) Yang, D.; Yang, Z.; Qin, W.; Zhang, Y.; Liu, S.; Li, C. Alternating precursor layer deposition for highly stable perovskite films towards efficient solar cells using vacuum deposition. *J. Mater. Chem. A* **2015**, *3*, 9401−9405.
(53) He, X.-L.; Liu, M.; Yang, G.-J.; Yao, H.-L.; Fan, S.-Q.; Li, C.-J. Photovoltaic performance degradation and recovery of the flexible dye-sensitized solar cells by bending and relaxing. *J. Power Sources* **2013**, *226*, 173−178.
(54) Kadro, J. M.; Nonomura, K.; Gachet, D.; Gratzel, M.; Hagfeldt, A. Facile route to freestanding $CH_3NH_3PbI_3$ crystals using inverse solubility. *Sci. Rep.* **2015**, *5*, 11654.

DOI: 10.1021/acsami.9b04373
ACS Appl. Mater. Interfaces 2019, 11, 17475−17481